Cross sections and double-helicity asymmetries of midrapidity inclusive charged hadrons in $p + p$ collisions at $\sqrt{s} = 62.4$ GeV

A. Adare,[11] S. Afanasiev,[26] C. Aidala,[36] N. N. Ajitanand,[53] Y. Akiba,[47,48] H. Al-Bataineh,[42] J. Alexander,[53] K. Aoki,[30,47] L. Aphecetche,[55] J. Asai,[47] E. T. Atomssa,[31] R. Averbeck,[54] T. C. Awes,[43] B. Azmoun,[6] V. Babintsev,[21] M. Bai,[5] G. Baksay,[17] L. Baksay,[17] A. Baldisseri,[14] K. N. Barish,[7] P. D. Barnes,[33,*] B. Bassalleck,[41] A. T. Basye,[1] S. Bathe,[7] S. Batsouli,[43] V. Baublis,[46] C. Baumann,[37] A. Bazilevsky,[6] S. Belikov,[6,*] R. Bennett,[54] A. Berdnikov,[50] Y. Berdnikov,[50] A. A. Bickley,[11] J. G. Boissevain,[33] H. Borel,[14] K. Boyle,[54] M. L. Brooks,[33] H. Buesching,[6] V. Bumazhnov,[21] G. Bunce,[6,48] S. Butsyk,[33] C. M. Camacho,[33] S. Campbell,[54] B. S. Chang,[63] W. C. Chang,[2] J.-L. Charvet,[14] S. Chernichenko,[21] C. Y. Chi,[12] M. Chiu,[22] I. J. Choi,[63] R. K. Choudhury,[4] T. Chujo,[58] P. Chung,[53] A. Churyn,[21] V. Cianciolo,[43] Z. Citron,[54] B. A. Cole,[12] P. Constantin,[33] M. Csanád,[16] T. Csörgő,[62] T. Dahms,[54] S. Dairaku,[30,47] K. Das,[18] A. Datta,[36] G. David,[6] A. Denisov,[21] D. d'Enterria,[31] A. Deshpande,[48,54] E. J. Desmond,[6] O. Dietzsch,[51] A. Dion,[54] M. Donadelli,[51] O. Drapier,[31] A. Drees,[54] K. A. Drees,[5] A. K. Dubey,[61] A. Durum,[21] D. Dutta,[4] V. Dzhordzhadze,[7] Y. V. Efremenko,[43] F. Ellinghaus,[11] T. Engelmore,[12] A. Enokizono,[32] H. En'yo,[47,48] S. Esumi,[58] K. O. Eyser,[7] B. Fadem,[38] D. E. Fields,[41,48] M. Finger,[8] M. Finger, Jr.,[8] F. Fleuret,[31] S. L. Fokin,[29] Z. Fraenkel,[61,*] J. E. Frantz,[54] A. Franz,[6] A. D. Frawley,[18] K. Fujiwara,[47] Y. Fukao,[30,47] T. Fusayasu,[40] I. Garishvili,[56] A. Glenn,[11] H. Gong,[54] M. Gonin,[31] J. Gosset,[14] Y. Goto,[47,48] R. Granier de Cassagnac,[31] N. Grau,[12] S. V. Greene,[59] M. Grosse Perdekamp,[22,48] T. Gunji,[10] H.-Å. Gustafsson,[35,*] A. Hadj Henni,[55] J. S. Haggerty,[6] H. Hamagaki,[10] R. Han,[45] E. P. Hartouni,[32] K. Haruna,[20] E. Haslum,[35] R. Hayano,[10] X. He,[19] M. Heffner,[32] T. K. Hemmick,[54] T. Hester,[7] J. C. Hill,[25] M. Hohlmann,[17] W. Holzmann,[53] K. Homma,[20] B. Hong,[28] T. Horaguchi,[10,47,57] D. Hornback,[56] S. Huang,[59] T. Ichihara,[47,48] R. Ichimiya,[47] H. Iinuma,[30,47] Y. Ikeda,[58] K. Imai,[30,47] J. Imrek,[15] M. Inaba,[58] D. Isenhower,[1] M. Ishihara,[47] T. Isobe,[10,47] M. Issah,[53] A. Isupov,[26] D. Ivanischev,[46] B. V. Jacak,[54,†] J. Jia,[12] J. Jin,[12] B. M. Johnson,[6] K. S. Joo,[39] D. Jouan,[44] F. Kajihara,[10] S. Kametani,[47] N. Kamihara,[48] J. Kamin,[54] J. H. Kang,[63] J. Kapustinsky,[33] D. Kawall,[36,48] A. V. Kazantsev,[29] T. Kempel,[25] A. Khanzadeev,[46] K. M. Kijima,[20] J. Kikuchi,[60] B. I. Kim,[28] D. H. Kim,[39] D. J. Kim,[63] E. Kim,[52] S. H. Kim,[63] E. Kinney,[11] K. Kiriluk,[11] Á. Kiss,[16] E. Kistenev,[6] J. Klay,[32] C. Klein-Boesing,[37] L. Kochenda,[46] B. Komkov,[46] M. Konno,[58] J. Koster,[22] A. Kozlov,[61] A. Král,[13] A. Kravitz,[12] G. J. Kunde,[33] K. Kurita,[47,49] M. Kurosawa,[47] M. J. Kweon,[28] Y. Kwon,[56] G. S. Kyle,[42] R. Lacey,[53] Y. S. Lai,[12] J. G. Lajoie,[25] D. Layton,[22] A. Lebedev,[25] D. M. Lee,[33] K. B. Lee,[28] T. Lee,[52] M. J. Leitch,[33] M. A. L. Leite,[51] B. Lenzi,[51] X. Li,[9] P. Liebing,[48] T. Liška,[13] A. Litvinenko,[26] H. Liu,[42] M. X. Liu,[33] B. Love,[59] D. Lynch,[6] C. F. Maguire,[59] Y. I. Makdisi,[5] A. Malakhov,[26] M. D. Malik,[41] V. I. Manko,[29] E. Mannel,[12] Y. Mao,[45,47] L. Mašek,[8,24] H. Masui,[58] F. Matathias,[12] M. McCumber,[54] P. L. McGaughey,[33] N. Means,[54] B. Meredith,[22] Y. Miake,[58] P. Mikeš,[24] K. Miki,[58] A. Milov,[6] M. Mishra,[3] J. T. Mitchell,[6] A. K. Mohanty,[4] Y. Morino,[10] A. Morreale,[7] D. P. Morrison,[6] T. V. Moukhanova,[29] D. Mukhopadhyay,[59] J. Murata,[47,49] S. Nagamiya,[27] J. L. Nagle,[11] M. Naglis,[61] M. I. Nagy,[16] I. Nakagawa,[47,48] Y. Nakamiya,[20] T. Nakamura,[20] K. Nakano,[47,57] J. Newby,[32] M. Nguyen,[54] T. Niita,[58] R. Nouicer,[6] A. S. Nyanin,[29] E. O'Brien,[6] S. X. Oda,[10] C. A. Ogilvie,[25] M. Oka,[58] K. Okada,[48] Y. Onuki,[47] A. Oskarsson,[35] M. Ouchida,[20] K. Ozawa,[10] R. Pak,[6] A. P. T. Palounek,[33] V. Pantuev,[23,54] V. Papavassiliou,[42] J. Park,[52] W. J. Park,[28] S. F. Pate,[42] H. Pei,[25] J.-C. Peng,[22] H. Pereira,[14] V. Peresedov,[26] D. Yu. Peressounko,[29] C. Pinkenburg,[6] M. L. Purschke,[6] A. K. Purwar,[33] H. Qu,[19] J. Rak,[41] A. Rakotozafindrabe,[31] I. Ravinovich,[61] K. F. Read,[43,56] S. Rembeczki,[17] K. Reygers,[37] V. Riabov,[46] Y. Riabov,[46] D. Roach,[59] G. Roche,[34] S. D. Rolnick,[7] M. Rosati,[25] S. S. E. Rosendahl,[35] P. Rosnet,[34] P. Rukoyatkin,[26] P. Ružička,[24] V. L. Rykov,[47] B. Sahlmueller,[37] N. Saito,[30,47,48] T. Sakaguchi,[6] S. Sakai,[58] K. Sakashita,[47,57] V. Samsonov,[46] T. Sato,[58] S. Sawada,[27] K. Sedgwick,[7] J. Seele,[11] R. Seidl,[22] A. Yu. Semenov,[25] V. Semenov,[21] R. Seto,[7] D. Sharma,[61] I. Shein,[21] T.-A. Shibata,[47,57] K. Shigaki,[20] M. Shimomura,[58] K. Shoji,[30,47] P. Shukla,[4] A. Sickles,[6] C. L. Silva,[51] D. Silvermyr,[43] C. Silvestre,[14] K. S. Sim,[28] B. K. Singh,[3] C. P. Singh,[3] V. Singh,[3] M. Slunečka,[8] A. Soldatov,[21] R. A. Soltz,[32] W. E. Sondheim,[33] S. P. Sorensen,[56] I. V. Sourikova,[6] F. Staley,[14] P. W. Stankus,[43] E. Stenlund,[35] M. Stepanov,[42] A. Ster,[62] S. P. Stoll,[6] T. Sugitate,[20] C. Suire,[44] A. Sukhanov,[6] J. Sziklai,[62] E. M. Takagui,[51] A. Taketani,[47,48] R. Tanabe,[58] Y. Tanaka,[40] S. Taneja,[54] K. Tanida,[47,48,52] M. J. Tannenbaum,[6] A. Taranenko,[53] P. Tarján,[15] H. Themann,[54] T. L. Thomas,[41] M. Togawa,[30,47] A. Toia,[54] L. Tomášek,[24] Y. Tomita,[58] H. Torii,[20,47] R. S. Towell,[1] V-N. Tram,[31] I. Tserruya,[61] Y. Tsuchimoto,[20] C. Vale,[25] H. Valle,[59] H. W. van Hecke,[33] A. Veicht,[22] J. Velkovska,[59] R. Vértesi,[15] A. A. Vinogradov,[29] M. Virius,[13] V. Vrba,[24] E. Vznuzdaev,[46] X. R. Wang,[42] Y. Watanabe,[47,48] F. Wei,[25] J. Wessels,[37] S. N. White,[6] D. Winter,[12] C. L. Woody,[6] M. Wysocki,[11] W. Xie,[48] Y. L. Yamaguchi,[60] K. Yamaura,[20] R. Yang,[22] A. Yanovich,[21] J. Ying,[19] S. Yokkaichi,[47,48] G. R. Young,[43] I. Younus,[41] I. E. Yushmanov,[29] W. A. Zajc,[12] O. Zaudtke,[37] C. Zhang,[43] S. Zhou,[9] and L. Zolin[26]

(PHENIX Collaboration)

[1]*Abilene Christian University, Abilene, Texas 79699, USA*
[2]*Institute of Physics, Academia Sinica, Taipei 11529, Taiwan*
[3]*Department of Physics, Banaras Hindu University, Varanasi 221005, India*
[4]*Bhabha Atomic Research Centre, Bombay 400 085, India*
[5]*Collider-Accelerator Department, Brookhaven National Laboratory, Upton, New York 11973-5000, USA*
[6]*Physics Department, Brookhaven National Laboratory, Upton, New York 11973-5000, USA*
[7]*University of California-Riverside, Riverside, California 92521, USA*
[8]*Charles University, Ovocný trh 5, Praha 1, 116 36, Prague, Czech Republic*
[9]*Science and Technology on Nuclear Data Laboratory, China Institute of Atomic Energy, Beijing 102413, People's Republic of China*
[10]*Center for Nuclear Study, Graduate School of Science, University of Tokyo, 7-3-1 Hongo, Bunkyo, Tokyo 113-0033, Japan*
[11]*University of Colorado, Boulder, Colorado 80309, USA*
[12]*Columbia University, New York, New York 10027 and Nevis Laboratories, Irvington, New York 10533, USA*
[13]*Czech Technical University, Zikova 4, 166 36 Prague 6, Czech Republic*
[14]*Dapnia, CEA Saclay, F-91191, Gif-sur-Yvette, France*
[15]*Debrecen University, H-4010 Debrecen, Egyetem tér 1, Hungary*
[16]*ELTE, Eötvös Loránd University, H-1117 Budapest, Pázmány P. s. 1/A, Hungary*
[17]*Florida Institute of Technology, Melbourne, Florida 32901, USA*
[18]*Florida State University, Tallahassee, Florida 32306, USA*
[19]*Georgia State University, Atlanta, Georgia 30303, USA*
[20]*Hiroshima University, Kagamiyama, Higashi-Hiroshima 739-8526, Japan*
[21]*IHEP Protvino, State Research Center of Russian Federation, Institute for High Energy Physics, Protvino, 142281, Russia*
[22]*University of Illinois at Urbana-Champaign, Urbana, Illinois 61801, USA*
[23]*Institute for Nuclear Research of the Russian Academy of Sciences, prospekt 60-letiya Oktyabrya 7a, Moscow 117312, Russia*
[24]*Institute of Physics, Academy of Sciences of the Czech Republic, Na Slovance 2, 182 21 Prague 8, Czech Republic*
[25]*Iowa State University, Ames, Iowa 50011, USA*
[26]*Joint Institute for Nuclear Research, 141980 Dubna, Moscow Region, Russia*
[27]*KEK, High Energy Accelerator Research Organization, Tsukuba, Ibaraki 305-0801, Japan*
[28]*Korea University, Seoul, 136-701, Korea*
[29]*Russian Research Center "Kurchatov Institute," Moscow, 123098 Russia*
[30]*Kyoto University, Kyoto 606-8502, Japan*
[31]*Laboratoire Leprince-Ringuet, Ecole Polytechnique, CNRS-IN2P3, Route de Saclay, F-91128, Palaiseau, France*
[32]*Lawrence Livermore National Laboratory, Livermore, California 94550, USA*
[33]*Los Alamos National Laboratory, Los Alamos, New Mexico 87545, USA*
[34]*LPC, Université Blaise Pascal, CNRS-IN2P3, Clermont-Fd, 63177 Aubiere Cedex, France*
[35]*Department of Physics, Lund University, Box 118, SE-221 00 Lund, Sweden*
[36]*Department of Physics, University of Massachusetts, Amherst, Massachusetts 01003-9337, USA*
[37]*Institut für Kernphysik, University of Muenster, D-48149 Muenster, Germany*
[38]*Muhlenberg College, Allentown, Pennsylvania 18104-5586, USA*
[39]*Myongji University, Yongin, Kyonggido 449-728, Korea*
[40]*Nagasaki Institute of Applied Science, Nagasaki-shi, Nagasaki 851-0193, Japan*
[41]*University of New Mexico, Albuquerque, New Mexico 87131, USA*
[42]*New Mexico State University, Las Cruces, New Mexico 88003, USA*
[43]*Oak Ridge National Laboratory, Oak Ridge, Tennessee 37831, USA*
[44]*IPN-Orsay, Universite Paris Sud, CNRS-IN2P3, BP1, F-91406, Orsay, France*
[45]*Peking University, Beijing 100871, People's Republic of China*
[46]*PNPI, Petersburg Nuclear Physics Institute, Gatchina, Leningrad region, 188300, Russia*
[47]*RIKEN Nishina Center for Accelerator-Based Science, Wako, Saitama 351-0198, Japan*
[48]*RIKEN BNL Research Center, Brookhaven National Laboratory, Upton, New York 11973-5000, USA*
[49]*Physics Department, Rikkyo University, 3-34-1 Nishi-Ikebukuro, Toshima, Tokyo 171-8501, Japan*
[50]*Saint Petersburg State Polytechnic University, St. Petersburg, 195251 Russia*
[51]*Universidade de São Paulo, Instituto de Física, Caixa Postal 66318, São Paulo CEP05315-970, Brazil*
[52]*Seoul National University, Seoul, Korea*
[53]*Chemistry Department, Stony Brook University, SUNY, Stony Brook, New York 11794-3400, USA*
[54]*Department of Physics and Astronomy, Stony Brook University, SUNY, Stony Brook, New York 11794-3400, USA*
[55]*SUBATECH (Ecole des Mines de Nantes, CNRS-IN2P3, Université de Nantes) BP 20722-44307, Nantes, France*
[56]*University of Tennessee, Knoxville, Tennessee 37996, USA*
[57]*Department of Physics, Tokyo Institute of Technology, Oh-okayama, Meguro, Tokyo 152-8551, Japan*

[58]Institute of Physics, University of Tsukuba, Tsukuba, Ibaraki 305, Japan
[59]Vanderbilt University, Nashville, Tennessee 37235, USA
[60]Waseda University, Advanced Research Institute for Science and Engineering, 17 Kikui-cho, Shinjuku-ku, Tokyo 162-0044, Japan
[61]Weizmann Institute, Rehovot 76100, Israel
[62]Institute for Particle and Nuclear Physics, Wigner Research Centre for Physics, Hungarian Academy of Sciences (Wigner RCP, RMKI), H-1525 Budapest 114, P.O. Box 49, Budapest, Hungary
[63]Yonsei University, IPAP, Seoul 120-749, Korea

(Received 21 February 2012; published 8 November 2012)

Unpolarized cross sections and double-helicity asymmetries of single-inclusive positive and negative charged hadrons at midrapidity from $p + p$ collisions at $\sqrt{s} = 62.4$ GeV are presented. The PHENIX measurement of the cross sections for $1.0 < p_T < 4.5$ GeV/c are consistent with perturbative QCD calculations at next-to-leading order in the strong-coupling constant, α_s. Resummed pQCD calculations including terms with next-to-leading-log accuracy, yielding reduced theoretical uncertainties, also agree with the data. The double-helicity asymmetry, sensitive at leading order to the gluon polarization in a momentum-fraction range of $0.05 \lesssim x_{\text{gluon}} \lesssim 0.2$, is consistent with recent global parametrizations disfavoring large gluon polarization.

DOI: 10.1103/PhysRevD.86.092006 PACS numbers: 13.85.−t, 13.88.+e, 14.20.Dh

I. INTRODUCTION

The comparison of cross-section predictions with data on single-inclusive hadron production in hadronic collisions, $p + p \rightarrow h + X$, is important for understanding perturbative quantum chromodynamics (pQCD). For hadrons produced with transverse momenta $p_T \gg \Lambda_{\text{QCD}}$, the cross section factorizes into a convolution involving long-distance and short-distance components [1,2]. Long-distance components include universal parton distribution functions (PDFs) describing the partonic structure of the initial hadrons and fragmentation functions (FFs) for the final-state hadron. The short-distance part describes the hard scattering of partons. The long-distance components, PDFs and FFs, can be extracted from other processes, such as deep-inelastic scattering and hadron production in e^+e^- colliders. This allows for a test of the short-distance part of the convolution, which can be estimated using pQCD. In particular, differences between data and predictions can indicate the importance of neglected higher-order terms in the expansion or power-suppressed contributions [3].

Next-to-leading-order (NLO) pQCD and collinear factorization successfully describe cross-section measurements at a center-of-mass energy ($\sqrt{s}$) of 200 GeV for midrapidity neutral pions [4,5], jets [6–8], and direct photons [9], as well as forward rapidity pions and kaons [10,11]. However, at lower $\sqrt{s}$, in particular, in fixed-target experiments [12–15] with $20 \lesssim \sqrt{s} \lesssim 40$ GeV, NLO pQCD calculations significantly underpredict hadron production, by factors of three or more [3]. The consistency between NLO estimations and data at low $\sqrt{s}$ was improved [3,16,17] by including the resummation of large logarithmic corrections to the partonic cross section to all orders in the strong coupling α_s. The corrections are of the form $\alpha_s^k \ln^{2k}(1 - \hat{x}_T^2)$ for the kth-order term in the perturbative expansion. Here $\hat{x}_T \equiv 2\hat{p}_T/\sqrt{\hat{s}}$, where $\hat{p}_T = p_T/z$ is the transverse momentum of the parton fragmenting into the observed hadron with a fraction z of the parton transverse momentum, and $\sqrt{\hat{s}} = \sqrt{x_1 x_2 s}$ is the partonic center-of-mass energy where x_1, x_2 are momentum fractions carried by two interacting partons. The corrections are especially relevant in the threshold regime $\hat{x}_T \rightarrow 1$ in which the initial partons have just enough energy to produce a high-transverse-momentum parton fragmenting into the observed hadron. In this regime gluon bremsstrahlung is suppressed, and these corrections are large [16]. However, the addition of the resummed next-to-leading-log (NLL) terms to an NLO calculation may not provide the best means of describing data in a given kinematic region, for example, when the (unknown) higher-order terms that are omitted from the calculation have comparable magnitude and opposite sign to the NLL terms. It is therefore important to test pQCD calculations against data in a region of intermediate $\sqrt{s}$, to better define the kinematic ranges over which pQCD calculations can be applied with confidence.

The data presented here from the PHENIX detector at the Relativistic Heavy Ion Collider (RHIC) for the production of nonidentified, long-lived charged hadrons ($\pi^{\pm}$, $K^{\pm}$, $p^{\pm}$)—loosely termed as inclusive charged hadrons–make use of approximately 5 times the geometric detector acceptance and different detection techniques compared to the identified-charged-hadron analysis [18], which depended on the time-of-flight detector at PHENIX. The new results allow tests of NLO and NLL predictions based on a separate measurement in a wider p_T range and with higher statistics. In addition, the theoretical calculations make use of inclusive-charged-hadron fragmentation functions [19], parametrized independently from those for the identified charged hadrons [20]. Alternatively, assuming

*Deceased.
†PHENIX Spokesperson: jacak@skipper.physics.sunysb.edu

the reliability of the short-distance aspects of the theory, the data may be used to refine knowledge of fragmentation functions. The present measurements cover a greater p_T range than the identified charged-hadron cross sections, where the measured momentum ranges for pions, kaons, and protons are 0.3–3 GeV/c, 0.4–2 GeV/c, and 0.5–4.5 GeV/c, respectively [18]. These cross-section measurements of nonidentified charged hadrons are also important as baselines for extracting nuclear modification factors in high-p_T hadron production in heavy ion collisions at RHIC [21,22].

The charged hadrons in these measurements were produced from collisions of transversely- and longitudinally polarized proton beams, a unique capability of RHIC [23]. While the cross-section measurements discussed above require averaging over the beam polarizations, sorting the hadron yields by colliding proton helicities (for longitudinal beam polarizations) provides sensitivity to the helicity PDFs [24]. The ability to probe helicity PDFs is essential for understanding the spin structure of the proton [25].

The spin of the proton originates from the spin and orbital angular momenta of its quark, antiquark, and gluon constituents. The contribution carried by quark and antiquark spin, determined from polarized deep-inelastic scattering (pDIS) experiments [26–36] using polarized leptons and polarized nucleons, is ~25%–35% [25,37–41]. This is surprisingly small [25] and implies that the majority of the spin of the proton must originate from gluon spin and/or orbital angular momentum.

Colliding longitudinally polarized proton beams provides sensitivity to the gluon-helicity distribution function at leading order. The helicity-dependent difference in hadron production is defined as

$$\frac{d\Delta\sigma}{dp_T} \equiv \frac{1}{2}\left[\frac{d\sigma^{++}}{dp_T} - \frac{d\sigma^{+-}}{dp_T}\right],$$

where the superscripts $++$ and $+-$ refer to the same- and opposite-helicity combinations of the colliding protons [24]. Factorization allows this to be written as a convolution of the long- and short-distance terms summed over all possible flavors for the partonic interaction $a + b \to c + X'$, where c fragments into the detected hadron h:

$$\frac{d\Delta\sigma}{dp_T} = \sum_{abc} \int dx_a dx_b dz_c \Delta f_a(x_a, \mu_f)\Delta f_b(x_b, \mu_f) \times \frac{d\Delta\hat{\sigma}^{ab\to cX'}}{dp_T}(x_a P_a, x_b P_b, P^h/z_c, \mu_f, \mu'_f, \mu_r) \times D_c^h(z_c, \mu'_f), \quad (1)$$

where $\Delta f(x, \mu_f)$ are the polarized PDFs of the colliding partons carrying light-cone momentum fraction x evaluated at factorization scale μ_f. The fragmentation function of scattered parton c into hadron h with fraction z_c of the scattered parton momentum is $D_c^h(z_c, \mu'_f)$ at fragmentation scale μ'_f. The helicity-dependent difference in the cross section of the hard partonic scattering $a + b \to c + X'$ is denoted by $d\Delta\hat{\sigma}$ and is calculable in perturbative QCD. Cross-section calculations to finite order in α_s have a dependence on factorization and renormalization scales μ_f and μ_r.

Instead of directly measuring the helicity-dependent cross-section difference $d\Delta\sigma/dp_T$, we extract the double-longitudinal spin asymmetry defined as the ratio of the polarized to unpolarized cross sections $A_{LL} \equiv d\Delta\sigma/d\sigma$. Here, $d\sigma$ is the helicity-averaged (unpolarized) cross section $d\sigma \equiv [d\sigma^{++} + d\sigma^{+-}]/2$. The ratio $d\Delta\sigma/d\sigma$ has smaller systematic uncertainties since some of the uncertainties cancel.

At $\sqrt{s} = 62.4$ GeV, the production of final-state hadrons at midrapidity in a transverse-momentum range $1.5 \le p_T \le 4.5$ GeV/c is dominated by quark-gluon scattering [42]. This makes the asymmetry reported here, $A_{LL}(p + p \to h^{\pm} + X)$, sensitive to the polarized gluon PDF $\Delta G(x)$ at leading order, and more sensitive to its sign than processes dominated by gluon-gluon scattering or that produce isospin-symmetric particles. For example, preferential fragmentation of up quarks into positive pions and down quarks into negative pions, combined with the fact that the up quark helicity PDF is positive and the down quark helicity PDF is negative, would lead to an ordering of the asymmetries of pions (charged and neutral) directly sensitive to the sign of the gluon-helicity PDF. Positive $\Delta G(x)$ would lead to $A_{LL}^{\pi^+} \ge A_{LL}^{\pi^0} \ge A_{LL}^{\pi^-}$, whereas a negative $\Delta G(x)$ would imply an opposite ordering. These results can be combined with data from polarized-collider and fixed-target experiments in a global analysis to reduce uncertainties on the gluon-helicity distribution by de Florian-Sassot-Stratmann-Vogelsang (DSSV) [43,44].

II. EXPERIMENTAL SETUP

This analysis uses the PHENIX central arm spectrometers. Each arm has an acceptance covering a pseudorapidity range $|\eta| < 0.35$ and $\Delta\phi = \frac{\pi}{2}$ in azimuth [45,46]. The PHENIX central magnet creates an axial magnetic field with $\int Bdl = 0.78$ T · m at $\frac{\pi}{2}$ in this region.

Midrapidity charged hadrons are tracked in the drift chambers (DC), which are located outside the magnetic field with an inner radius of 2.0 m and outer radius of 2.4 m. The tracks are reconstructed as nearly straight lines and yield the deflection in the axial magnetic field to determine the transverse momentum with a resolution $\frac{dp_T}{p_T} = 0.007 \oplus 0.009 p_T$ (GeV/c) [47]. The first term in the resolution is dominated by multiple scattering in material before the DC, while the second arises from the finite angular resolution of the DC. The momentum scale is set by requiring the proton mass reconstructed from the measured momentum and time of flight to match the known proton mass.

Track reconstruction also utilizes two layers of pad chambers (PC), which are multiwire proportional chambers with pad readouts [46]. The first layer, PC1, is located after the DC, with an average radius of 2.49 m. PC1 information is used in conjunction with the DC hits and vertex information to determine the polar angle for each charged track. The outermost layer PC3 is at an average radius of 4.98 m and is used for charged track selection by matching PC3 hit positions with track projections on it using information from the DC and PC1 and the measured event vertex. Matching track projections with hit positions in PC3 also helps in rejecting decay backgrounds from primary hadrons.

Vertex and timing information is provided by two beam-beam counters (BBCs) [45] placed around the beam pipe. The BBCs are located 1.44 m forward and backward of the nominal interaction point. Each BBC comprises an array of 64 phototubes fitted with 3 cm long quartz radiators. The phototubes detect Čerenkov radiation from charged particles traversing the quartz. The detectors cover a pseudorapidity range of $3.0 \leq |\eta| \leq 3.9$, and a full $\Delta\phi = 2\pi$ in azimuth. A coincidence of hits from the two BBCs forms the minimum bias trigger, with timing information providing the location of the event vertex along the beam line with a few cm precision.

To eliminate the $e^{\pm}$ background due to photon conversion in material before the DC (primarily the beam pipe and DC entrance window), the analysis uses information from a ring imaging Čerenkov detector (RICH) [46] located after the DC. The RICH uses CO_2 at atmospheric pressure as a radiator, with a momentum threshold of 17 MeV/c for $e^{\pm}$ and 4.7 GeV/c for charged pions. A RICH veto (ensuring no RICH hits) is used to reject $e^{\pm}$ and results in an upper transverse-momentum limit of $p_T < 4.5$ GeV/c for charged hadrons in the analysis.

Zero degree calorimeters (ZDC), which detect neutral particles near the beam pipe ($\theta < 2.5$ mrad), are used in conjunction with the BBC to estimate the systematic uncertainty on the relative luminosity for the asymmetry measurements [48]. The BBC and ZDC are also used to determine the integrated luminosity measurement [49,50].

The stable spin direction of polarized protons in RHIC is vertical. The spin direction can be rotated into the longitudinal direction at the PHENIX interaction region using pairs of spin rotators. The polarizations of the beams at RHIC are measured every few hours by carbon target polarimeters [51], which are normalized to an absolute measurement with a hydrogen jet target polarimeter [52].

III. CROSS SECTION

The results presented here are the first measurements of the cross section of inclusive charged-hadron production at midrapidity in the transverse-momentum range $0.5 \leq p_T \leq 4.5$ GeV/c from $p + p$ collisions at $\sqrt{s} = 62.4$ GeV. The analysis techniques are similar to methods described in Ref. [53] and are briefly explained in Sec. III A. The cross-section results are presented and discussed in Sec. III B.

A. Cross-section measurement

Approximately 2.14×10^8 BBC-triggered events corresponding to an integrated luminosity of 15.6 nb^{-1} from polarization-averaged $p + p$ data taken in 2006 have been analyzed. We calculate the midrapidity charged-hadron production cross section using the following formula:

$$\frac{E}{c}\frac{d^3\sigma}{dp^3} = \frac{\sigma_{\mathrm{BBC}}}{N_{\mathrm{BBC}}}\frac{d^3N(p_T)}{d\phi p_T dp_T dy} R_{\mathrm{smear}} C_{\mathrm{trig}} \frac{1}{E_{\mathrm{eff}}^{\mathrm{acc}}}, \quad (2)$$

where $\sigma_{\mathrm{BBC}}W$ is the $p + p$ cross section seen by the BBC as measured in Ref. [48], N_{BBC} is the total number of BBC-triggered events analyzed, R_{smear} is the correction factor for the smearing of track p_T owing to the momentum resolution of the detectors as well as multiple scattering of the hadron tracks, C_{trig} is the correction factor for BBC trigger bias, and $E_{\mathrm{eff}}^{\mathrm{acc}}$ is the combined correction factor for geometrical acceptance of the detectors and reconstruction efficiency.

The reconstructed charged tracks in the transverse-momentum range $0.5 \leq p_T \leq 4.5$ GeV/c from events with vertices within ± 30 cm of the nominal interaction point are matched to projected hit positions in PC3 in azimuthal (ϕ) and beam direction (z). Distributions of the matching variables (difference between the projected track position and actual hits on PC3, termed PC3dϕ and PC3dz) are fit with the combination of a signal Gaussian and a second Gaussian for background. Figure 1 demonstrates the method for a sample p_T bin. The width of the fit to the signal distribution is used to impose a simultaneous selection window of 2σ for both matching variables.

The background to these measurements comes from several sources. One source is soft electrons from the magnet pole faces, and another is decays in flight of $\pi^{\pm}$

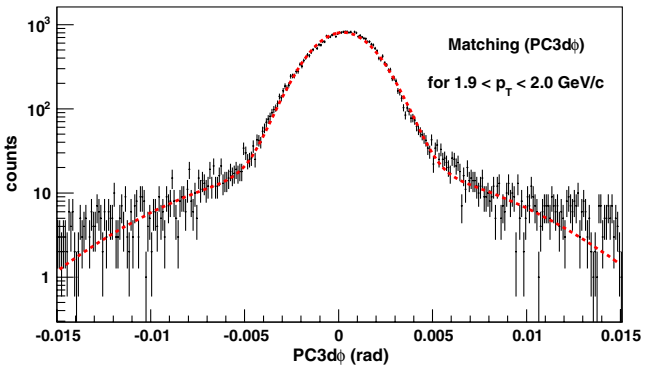

FIG. 1 (color online). Difference between the track-extrapolated and actual hit positions on PC3 in azimuth for a sample p_T bin. The histogram represents data; the dashed line represents a two-Gaussian fit.

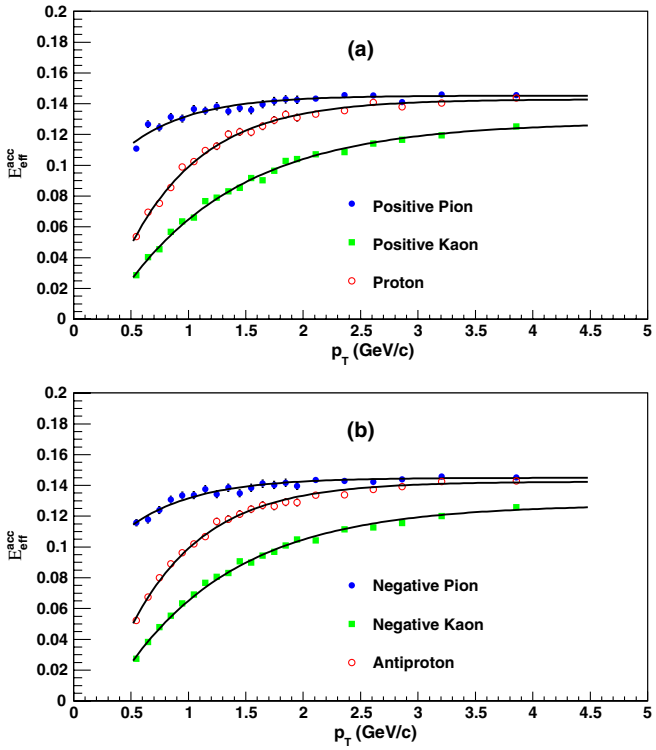

FIG. 2 (color online). Combined acceptance + detection efficiencies for (a) positive and (b) negative hadron species.

and $K^{\pm}$. Not all of these electrons are rejected by the RICH cut. Off-vertex electrons and daughter particles with a perpendicular momentum kick from the decay are reconstructed as apparent high-p_T tracks, but with wide Gaussian track matching distributions. The background fraction in each of the p_T bins is determined by using the distributions of the matching variables. Background fractions, which are 2%–5% for $p_T \leq 2.75$ GeV/c and ~30% in the highest p_T bin, are subsequently subtracted from hadron yields.

An additional source of background is the feed-down background produced by weak decays of mostly Λ particles close to the event vertex with apparent momenta close to their true momenta and matching distributions peaked under the signal. The decays $\Lambda \rightarrow p\pi^-$, $\Sigma^+ \rightarrow p\pi^0$ and Λ production from Σ^0, Ξ^0, Ξ^- are considered for feed-down contribution to protons (and the corresponding antiparticles for feed-down to antiprotons). Feed-down contributions to the detected protons and antiprotons from weak decays of Λ's and heavier hyperons are estimated using input Λ and $\bar{\Lambda}$ spectra from $p + p$ measurements at $\sqrt{s} = 63$ GeV at the Intersecting Storage Rings (ISR) [54,55] and at $\sqrt{s} = 62.4$ GeV at PHENIX with a GEANT3-based [56] simulation of the PHENIX detector. Details of the feed-down calculations are described in [48]. The fractional contributions of the feed-down protons and antiprotons are independent of p_T above $p_T = 2$ GeV/c and are close to 7% and 15%, respectively. Below $p_T = 2$ GeV/c the fractions increase with decreasing p_T and are roughly 25% and 60% for protons and antiprotons, respectively, at $p_T = 0.5$ GeV/c.

Background-subtracted yields are corrected for angular resolution of the DC and for smearing of the reconstructed momenta resulting from multiple scattering of tracks, which depends on hadron mass. To account for the acceptance of the PHENIX detector system and the varying efficiency for different hadrons, single-particle Monte Carlo simulations are performed and are verified by comparing the live detector area between data and Monte Carlo simulation. Same hadron track selection criteria as used for the data are applied to the simulations and the appropriate correction factors are determined separately for each hadron species.

Figure 2 shows the efficiencies for the three positive hadron species. The small efficiency for kaons is due to decays in flight. The large decrease in efficiency at low p_T is due to the fact that the fixed pseudorapidity acceptance of the detector corresponds to a narrow range in rapidity for smaller p_T/m. The efficiencies are parametrized $(Ae^{Bp_T} + C)$ as a function of p_T. Table I shows the fit-function parameters. The fit values are used for the calculation of cross sections. Uncertainties of the fit parameters presented in Table I are not, however, used for determining the systematic uncertainty of the cross sections. Variation of the selection matching window is used to estimate systematic uncertainty of the cross sections due to these correction factors. The species-dependent corrections are applied according to their production fraction in the hadron mixture.

Figure 3 shows the production fractions, which were determined from identified hadron spectra from PHENIX [18], as well as from earlier data from the ISR [54]. The relative fractions were compared to those obtained from the NLO pQCD calculations described above and were

TABLE I. Fit-function parameters for the efficiency curves for different hadron species. See text for details.

Hadron	A	δA	B	δB	C	δC
π^+	−0.08	0.01	−1.8	0.2	0.145	0.001
K^+	−0.17	0.003	−0.97	0.03	0.128	0.001
p	−0.21	0.007	−1.54	0.05	0.143	0.001
π^-	−0.07	0.01	−1.7	0.2	0.145	0.001
K^-	−0.17	0.003	−1.01	0.03	0.128	0.001
p^-	−0.21	0.007	−1.56	0.05	0.142	0.001

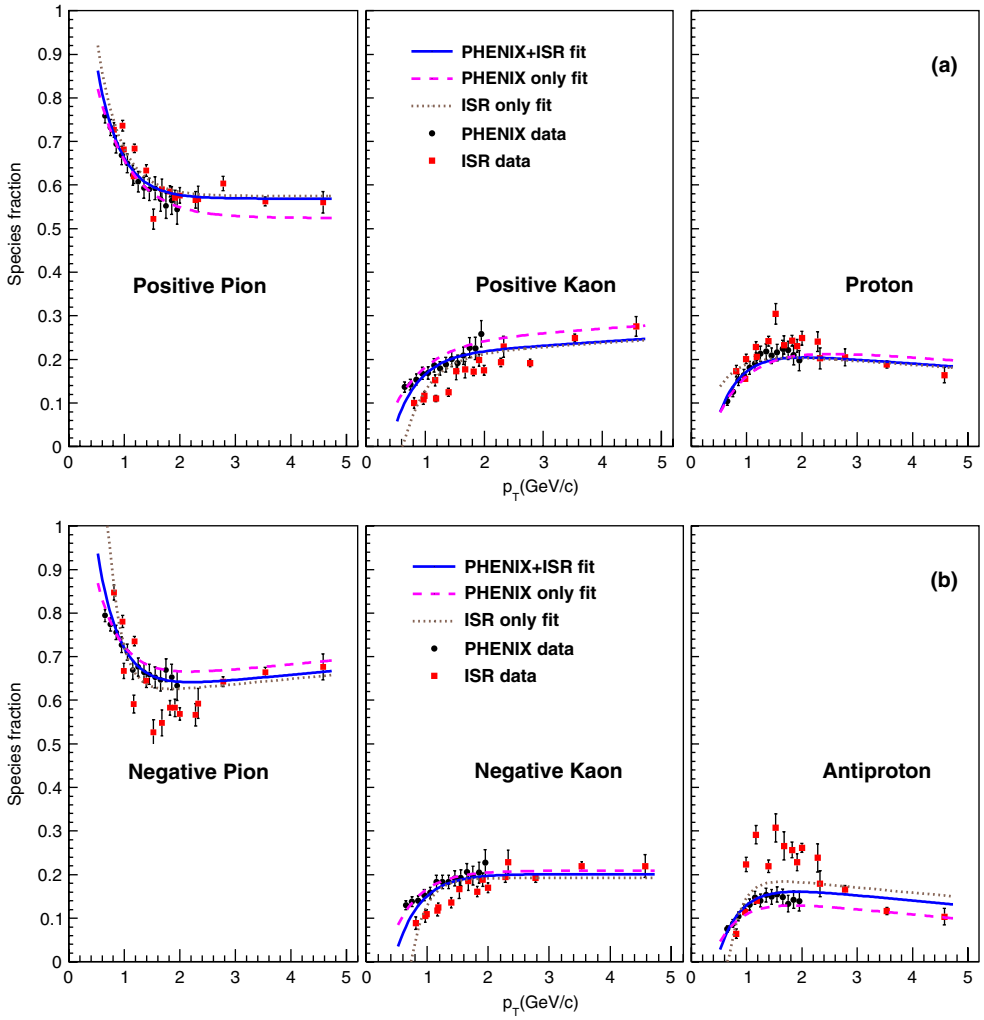

FIG. 3 (color online). Relative fraction of each species for (a) positive and (b) negative hadrons. The error bars on the data points are combined statistical and systematic uncertainties. The solid line represents a fit to both the PHENIX and ISR data. The dashed (dotted) line represents a fit to only the PHENIX (ISR) data.

found to be compatible within the uncertainty bands. The dotted and dashed lines in Fig. 2 represent fits with individual data sets. Parametrized fits of the form $Ae^{Bp_T} + C$ (for positive pions and negative kaons) and $Ae^{Bp_T} + C + Dp_T$ (for all other species) are performed under the constraint that the sum of the relative fractions is 1.

Table II gives the fit-function parameters. Relative fractions from the fit to both data sets combined (solid line) are used to apply the corrections for the measurements. The variation in the fit values for individual data sets (dotted and dashed lines), rather than the fit parameter uncertainties from Table II, are used to estimate systematic uncertainty of the cross-section measurements due to this quantity. The corrected yields are scaled by the BBC trigger bias, as described in Ref. [48].

Acceptance and efficiency factors are determined by generating single-particle events with uniform transverse momentum and rapidity distributions with a vertex distribution

TABLE II. Fit-function parameters for relative fractions of different species in the hadron mix. See text for details.

Hadron	A	δA	B	δB	C	δC	D	δD
π^+	1.02	0.56	−2.39	0.41	0.57	0.26	···	···
K^+	−0.53	0.56	−2.39	0.41	0.20	0.23	0.009	0.001
p	−0.49	1.12	−2.39	0.41	0.23	0.49	−0.009	0.001
π^-	1.17	0.56	−2.49	0.41	0.61	0.26	0.012	0.001
K^-	−0.61	0.56	−2.49	0.41	0.20	0.23	···	···
p^-	−0.56	1.12	−2.49	0.41	0.18	0.49	−0.012	0.001

TABLE III. Systematic uncertainties of cross-section measurements from various sources.

Source	Systematic uncertainty
Acceptance and efficiency correction	11%–24%
σ_{BBC}	11%
Trigger bias	2.5%
Monte Carlo/data scale factor	2%
PID fraction	1%–5%
Background fraction	1%–5%
Momentum smearing correction	1%–2%

closely resembling that in the data. The effect of the smearing of detected hadron spectra due to momentum resolution of the detector is determined separately. Identified hadron spectra from the ISR [54], as a function of p_T, are converted into yields in bins of bending angle α ($\alpha = \frac{\kappa}{p_T}$, where $K = 101$ mrad GeV/c) in the DC. The resulting distributions are smeared with the angular resolution $\delta\alpha = 0.9 + 0.007\alpha$, where the first term is the angular resolution of the DC and the α-dependent term incorporates the effects of multiple scattering. Smeared distributions are converted back to cross sections as functions of p_T, and the ratio of smeared to original spectra is used as the correction factor due to momentum smearing. Variation of angular resolution is used to determine the systematic uncertainty of the cross section due to this correction factor.

The integrated luminosity $\mathcal{L}_{\mathrm{int}} = \frac{N_{\mathrm{BBC}}}{\sigma_{\mathrm{BBC}}}$, required for normalization of the invariant cross section, is calculated using the count of BBC-triggered events and the BBC normalization parameter σ_{BBC}. The parameter σ_{BBC} is the $p + p$ cross section seen by the BBC and is measured by the Van der Meer (Vernier) scan technique [50]. The quantity $\sigma_{\mathrm{BBC}} = 13.7 \pm 1.5$ (syst) mb for the relevant data set has been measured for previous PHENIX results and was discussed in detail in Ref. [48].

Table III shows the systematic uncertainties of cross-section measurements from various sources. The largest contribution (11%–24%) to the p_T-dependent systematic uncertainty comes from the correction for the acceptance and detection efficiencies. The uncertainty on the cross section due to this correction factor is determined by varying the selection parameters in the MC simulations. The trigger bias introduces a 2.5% uncertainty in the overall normalization, in addition to the 11% uncertainty on σ_{BBC}. Determination of the background fraction and the production fraction of separate hadron species each introduces a 1%–5% p_T-dependent systematic uncertainty. Uncertainties from other sources, for example, the correction for momentum resolution, the correction for the active area of the detector in experiment and Monte Carlo simulation, are ~1%–2%.

B. Cross-section results

Figure 4 and Table IV show the inclusive charged-hadron cross sections from $p + p$ collisions at $\sqrt{s} = 62.4$ GeV as a function of p_T. A combined p_T-independent normalization uncertainty of 11.2% (uncertainties in the measurements of σ_{BBC} and BBC trigger bias) is not shown.

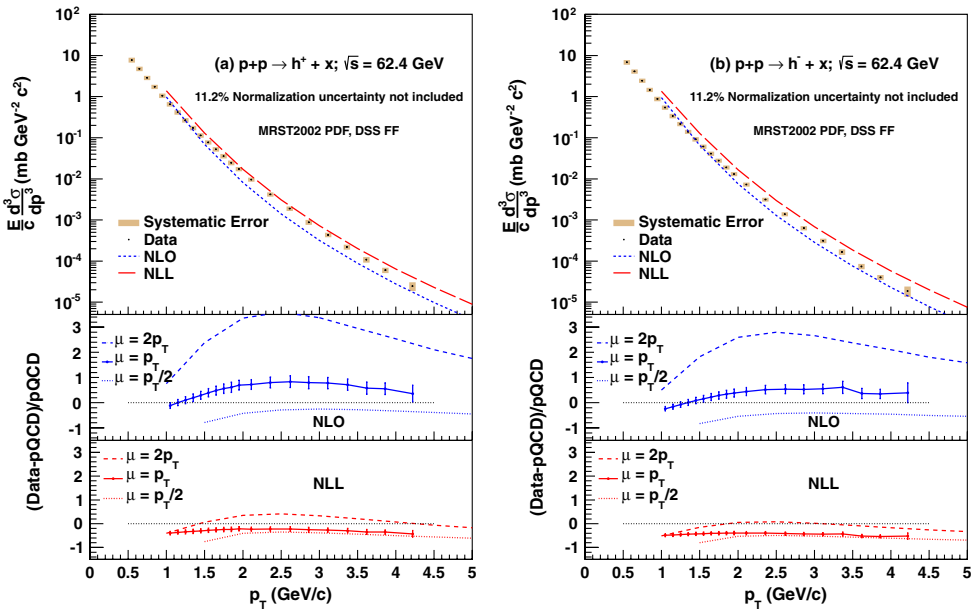

FIG. 4 (color online). Cross section of inclusive-charged-hadron production at midrapidity in $p + p$ at 62.4 GeV for (a) positive and (b) negative hadrons. NLO and NLL theoretical predictions [57] at midrapidity, using MRST2002 parton distribution functions [58] and DSS fragmentation functions [19], at factorization, renormalization, and fragmentation scale $\mu = p_T$ are shown as curves. The lower panels show the scale dependence of the NLO and NLL results.

TABLE IV. Cross section of midrapidity charged-hadron production from $p + p$ collisions at $\sqrt{s} = 62.4$ GeV as a function of p_T. The errors represent the statistical (first) and systematic uncertainties. The data are corrected for the contribution of feed-down protons and antiprotons. A normalization uncertainty of 11.2% is not included.

p_T (GeV/c)	h^+ mb GeV^{-2} c^2	h^- mb GeV^{-2} c^2
0.55	$7.80 \pm 1.2 \times 10^{-03} \pm 1.1$	$6.87 \pm 1.1 \times 10^{-03} \pm 9.3 \times 10^{-01}$
0.65	$4.78 \pm 8.7 \times 10^{-04} \pm 5.9 \times 10^{-01}$	$4.10 \pm 8.0 \times 10^{-04} \pm 5.0 \times 10^{-01}$
0.75	$2.87 \pm 6.3 \times 10^{-04} \pm 3.5 \times 10^{-01}$	$2.45 \pm 5.7 \times 10^{-04} \pm 2.9 \times 10^{-01}$
0.85	$1.73 \pm 4.6 \times 10^{-04} \pm 2.1 \times 10^{-01}$	$1.46 \pm 4.2 \times 10^{-04} \pm 1.7 \times 10^{-01}$
0.95	$1.06 \pm 3.4 \times 10^{-04} \pm 1.3 \times 10^{-01}$	$8.83 \times 10^{-01} \pm 3.1 \times 10^{-04} \pm 1.1 \times 10^{-01}$
1.05	$6.55 \times 10^{-01} \pm 2.5 \times 10^{-04} \pm 8.2 \times 10^{-02}$	$5.43 \times 10^{-01} \pm 2.3 \times 10^{-04} \pm 6.6 \times 10^{-02}$
1.15	$4.18 \times 10^{-01} \pm 1.9 \times 10^{-04} \pm 5.2 \times 10^{-02}$	$3.40 \times 10^{-01} \pm 1.7 \times 10^{-04} \pm 4.1 \times 10^{-02}$
1.25	$2.67 \times 10^{-01} \pm 1.5 \times 10^{-04} \pm 3.4 \times 10^{-02}$	$2.16 \times 10^{-01} \pm 1.3 \times 10^{-04} \pm 2.6 \times 10^{-02}$
1.35	$1.73 \times 10^{-01} \pm 1.2 \times 10^{-04} \pm 2.2 \times 10^{-02}$	$1.41 \times 10^{-01} \pm 1.0 \times 10^{-04} \pm 1.6 \times 10^{-02}$
1.45	$1.14 \times 10^{-01} \pm 9.0 \times 10^{-05} \pm 1.4 \times 10^{-02}$	$9.21 \times 10^{-02} \pm 8.0 \times 10^{-05} \pm 1.1 \times 10^{-02}$
1.55	$7.73 \times 10^{-02} \pm 7.2 \times 10^{-05} \pm 9.3 \times 10^{-03}$	$6.11 \times 10^{-02} \pm 6.3 \times 10^{-05} \pm 7.2 \times 10^{-03}$
1.65	$5.25 \times 10^{-02} \pm 5.7 \times 10^{-05} \pm 6.4 \times 10^{-03}$	$4.11 \times 10^{-02} \pm 5.0 \times 10^{-05} \pm 4.7 \times 10^{-03}$
1.75	$3.59 \times 10^{-02} \pm 4.6 \times 10^{-05} \pm 4.4 \times 10^{-03}$	$2.79 \times 10^{-02} \pm 4.0 \times 10^{-05} \pm 3.3 \times 10^{-03}$
1.85	$2.46 \times 10^{-02} \pm 3.7 \times 10^{-05} \pm 3.1 \times 10^{-03}$	$1.90 \times 10^{-02} \pm 3.2 \times 10^{-05} \pm 2.2 \times 10^{-03}$
1.95	$1.74 \times 10^{-02} \pm 3.0 \times 10^{-05} \pm 2.0 \times 10^{-03}$	$1.31 \times 10^{-02} \pm 2.6 \times 10^{-05} \pm 1.5 \times 10^{-03}$
2.11	$9.61 \times 10^{-03} \pm 1.4 \times 10^{-05} \pm 1.1 \times 10^{-03}$	$7.32 \times 10^{-03} \pm 1.2 \times 10^{-05} \pm 8.3 \times 10^{-04}$
2.36	$4.19 \times 10^{-03} \pm 8.5 \times 10^{-06} \pm 5.0 \times 10^{-04}$	$3.14 \times 10^{-03} \pm 7.3 \times 10^{-06} \pm 3.5 \times 10^{-04}$
2.61	$1.89 \times 10^{-03} \pm 5.5 \times 10^{-06} \pm 2.4 \times 10^{-04}$	$1.38 \times 10^{-03} \pm 4.6 \times 10^{-06} \pm 1.6 \times 10^{-04}$
2.86	$8.80 \times 10^{-04} \pm 3.6 \times 10^{-06} \pm 1.2 \times 10^{-04}$	$6.36 \times 10^{-04} \pm 3.0 \times 10^{-06} \pm 7.5 \times 10^{-05}$
3.11	$4.33 \times 10^{-04} \pm 2.4 \times 10^{-06} \pm 5.4 \times 10^{-05}$	$3.12 \times 10^{-04} \pm 2.0 \times 10^{-06} \pm 3.8 \times 10^{-05}$
3.37	$2.20 \times 10^{-04} \pm 1.6 \times 10^{-06} \pm 2.9 \times 10^{-05}$	$1.67 \times 10^{-04} \pm 1.4 \times 10^{-06} \pm 2.5 \times 10^{-05}$
3.62	$1.09 \times 10^{-04} \pm 1.1 \times 10^{-06} \pm 1.7 \times 10^{-05}$	$7.41 \times 10^{-05} \pm 9.1 \times 10^{-07} \pm 1.1 \times 10^{-05}$
3.87	$6.03 \times 10^{-05} \pm 8.1 \times 10^{-07} \pm 9.0 \times 10^{-06}$	$4.02 \times 10^{-05} \pm 6.4 \times 10^{-07} \pm 5.5 \times 10^{-06}$
4.22	$2.46 \times 10^{-05} \pm 3.5 \times 10^{-07} \pm 6.0 \times 10^{-06}$	$1.88 \times 10^{-05} \pm 2.9 \times 10^{-07} \pm 5.3 \times 10^{-06}$

In the overlapping p_T range, the results were found to be consistent with the species-combined (pion + kaon + (anti)proton) cross sections from identified results at PHENIX [18] as well as ISR results at $\sqrt{s} = 63$ GeV [54]. On the upper panels of both plots in Fig. 4, cross sections are compared to NLO and NLL calculations at a factorization, renormalization, and fragmentation scale of $\mu = p_T$ [57]. The calculations were performed using Martin-Roberts-Stirling-Thorne (MRST2002) PDFs [58] and de Florian-Sassot-Stratmann (DSS) fragmentation functions [19]. The NLO predictions have been shown to describe midrapidity cross-section results for neutral pions [59,60] and charged hadrons [53] at $\sqrt{s} = 200$ GeV within ~20% for a scale choice of $\mu = p_T$. For the present results at $\sqrt{s} = 62.4$ GeV, the NLO calculations underpredict the data by as much as ~80% in the case of positive hadrons and ~60% in the case of negative hadrons for the same scale choice. However, the NLO calculations have a large scale dependence and are consistent with the data after taking the scale uncertainties into account. The lower two panels in the Fig. 4 plots show the dependence of the theoretical calculations on the choice of the factorization, renormalization, and fragmentation scale (μ) for three different values (p_T, $p_T/2$, and $2p_T$). The inclusion of higher-order terms in the NLL calculations leads to a considerably smaller scale dependence.

These new data at an energy intermediate to typical fixed-target and collider energies are timely, as the details of how to work with resummation techniques in different kinematic regimes are currently being explored by the theoretical community (see, for example, [3,16,17]). Comparison of the present results to the calculations at NLO with and without NLL terms included indicates that in the measured kinematic range, NLL terms make relevant contributions to the cross section. However, the tendency of the NLL calculations to overpredict the data, by as much as ~40% in the case of positive hadrons and ~50% in the case of negative hadrons for a scale choice of p_T, may indicate that there are terms in the full next-to-next-to-leading-order (NNLO) expansion that are of comparable magnitude and opposite sign to those in the NLL calculation. These measurements corroborate similar indications from neutral pion cross-section results [48] and identified hadron cross-section results [18] at PHENIX. The present measurements can also be useful in a future determination of inclusive charged-hadron fragmentation functions, as progress in pQCD has allowed inclusion of $p + p$ cross-section measurements and semi-inclusive deep-inelastic lepton-nucleon scattering data in FF parametrizations along with the traditionally used e^+e^- data since 2007 [19,20,61].

IV. DOUBLE-HELICITY ASYMMETRY

We measured the double-helicity asymmetries, A_{LL}, of inclusive positive and negative hadron production in the transverse-momentum range of $0.5 \leq p_T \leq 4.5$ GeV/c at midrapidity from longitudinally polarized $p + p$ collisions at $\sqrt{s} = 62.4$ GeV.

A. A_{LL} measurement

The double-helicity asymmetry of charged hadrons is defined as the relative difference between hadron production cross sections from collisions of the same- and opposite-helicity state protons. Experimentally, the asymmetry is measured as

$$A_{LL} = \frac{1}{P_B \cdot P_Y} \frac{N_{++} - R \cdot N_{+-}}{N_{++} + R \cdot N_{+-}}, \tag{3}$$

where P_B, P_Y are polarizations of the two colliding beams in RHIC (termed "blue" and "yellow"), N_{++}, N_{+-} are the midrapidity hadron yields from collisions of the same- and opposite-helicity protons, and relative luminosity $R = \frac{L_{++}}{L_{+-}}$ is the ratio of luminosity of the same-helicity collisions to that of opposite-helicity collisions.

For the 2006 $p + p$ data set at $\sqrt{s} = 62.4$ GeV, the luminosity-weighted average beam polarizations for both beams are measured to be $\langle P \rangle = 0.48$, and the average magnitude of the product of polarization of the two beams is $\langle P_B \cdot P_Y \rangle = 0.23$ with a relative uncertainty of 13.9%. The colliding proton bunches at RHIC are assigned preset spin patterns repeated every four crossings. For consecutive fills with 120 bunches in the RHIC ring, four such different spin patterns are alternated in order to reduce false asymmetries and systematic effects of possible correlations between the detector response and the RHIC bunch structures.

Hadron counts are obtained under similar criteria as described for the cross-section measurements from the reconstructed tracks in Sec. III A. Approximately 1.63×10^8 BBC-triggered events with longitudinal beam polarization, corresponding to an integrated luminosity of 11.9 nb^{-1}, were analyzed for the asymmetry measurements. Luminosities for the same- and opposite-helicity events were obtained from crossing-by-crossing information of BBC trigger counts. The systematic uncertainty of the relative luminosity R, determined by comparing BBC-triggered events with events triggered by the ZDCs, was found to be 1.4×10^{-3}.

The asymmetry of the charged-hadron mixture is determined on a fill-by-fill basis and later combined statistically (luminosity-weighted average) to obtain the final results. No corrections were performed for the relative species fractions in the asymmetry analysis since asymmetries for the individual hadron species are not measured. The asymmetry of backgrounds from decays in flight, selected from the tail ends of the distribution of the matching variables (in beam direction z and azimuthal angle ϕ), is measured. The background asymmetry A_{LL}^{bkg} and background fraction are used to calculate the signal asymmetry and its statistical uncertainty. The feed-down from decays of Λ's and heavier hyperons, however, cannot be separated from hadron yields. The backgrounds from feed-down protons and antiprotons are a small contribution (1%–2.5%) to the total hadron yields given that pions dominate the hadron mixture, especially at low p_T. The asymmetry results are not corrected since the asymmetries of the feed-down backgrounds are unknown.

B. A_{LL} results

Figure 5 and Table V show the p_T dependence of the measured double-helicity asymmetries for inclusive-charged-hadron production at midrapidity in polarized

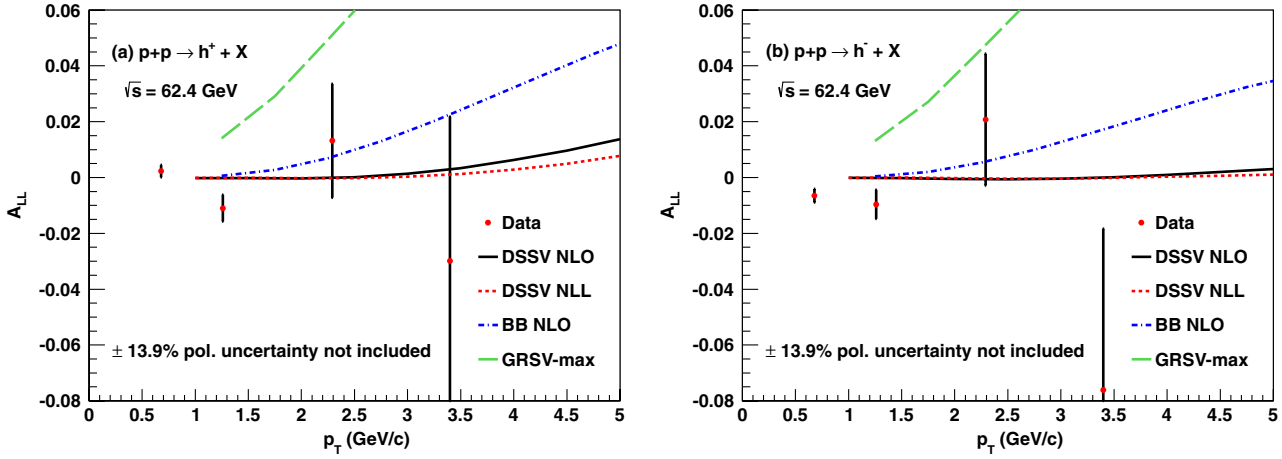

FIG. 5 (color online). Double-helicity asymmetry (A_{LL}) of (a) positive and (b) negative charged-hadron production from polarized $p + p$ collisions at $\sqrt{s} = 62.4$ GeV. The results are compared to NLO and NLL pQCD predictions using several parametrizations of the helicity PDFs (see text for details).

TABLE V. The double-helicity asymmetries and the statistical uncertainties as a function of p_T for positive and negative inclusive charged hadrons from $p + p$ collisions at $\sqrt{s} = 62.4$ GeV. The fractional contribution to the yields from weak-decay feed-down to protons and antiprotons is shown; no correction to the asymmetries has been made for these contributions.

p_T (GeV/c)	$A_{LL} \pm \delta A_{LL}$ (h^+)	Estimated feed-down fraction (h^+)	$A_{LL} \pm \delta A_{LL}$ (h^-)	Estimated feed-down fraction (h^-)
0.68	0.0023 ± 0.0022	0.022	-0.0065 ± 0.0024	0.021
1.26	-0.01096 ± 0.0048	0.016	-0.0096 ± 0.0052	0.025
2.29	0.0132 ± 0.0204	0.012	0.0208 ± 0.0236	0.021
3.40	-0.0299 ± 0.0517	0.011	-0.0761 ± 0.0578	0.018

$p + p$ collisions at $\sqrt{s} = 62.4$ GeV. The asymmetries are compared to NLO pQCD predictions[1] based on two different parametrizations of polarized PDFs at scale $\mu = p_T$.

The curves in Fig. 5 labeled "DSSV NLO" and "DSSV NLL" refer to calculations using DSSV parametrizations of the helicity PDFs [43]. The curves labeled "BB NLO" refer to calculations with Blümlein-Böttcher parametrizations of the helicity PDFs [38], and the "GRSV-max" curve refers to NLO pQCD calculations using Glück-Reya-Stratmann-Vogelsang parametrizations of the helicity PDFs assuming maximal saturation of the gluon polarization [$\Delta G(x, \mu^2) = G(x, \mu^2)$] [37]. DSSV calculations use MRST2002 unpolarized PDFs [58] whereas GRSV and BB calculations use unpolarized PDFs from the coordinated-theoretical-experimental project on QCD-6 [62]. However, within the present uncertainties, the effect due to different unpolarized PDFs is negligible. All of these pQCD calculations are performed using DSS fragmentation functions [19,20]. Polarized PDFs use fits to the pDIS data to extract parameters of the functional forms of PDFs. DSSV [43] parametrizations use RHIC data along with the available pDIS data to constrain the polarized PDFs. The asymmetries are also compared to the NLL estimations with the DSSV PDFs [57].

For the purpose of comparison with the experimental results, pQCD calculations were obtained for separate hadron species [pions, kaons, and (anti)protons] and were combined using their relative fractions (from pQCD calculations) in the hadron mixture and corresponding experimentally determined efficiency-acceptance factors (Fig. 2). Weighted averages of the calculated asymmetries of pions, kaons, and protons/antiprotons, with the product of the corresponding relative fraction and the efficiency-acceptance factor as the weight, are compared to the measurements. The measured asymmetries are small and consistent with zero. The results are also consistent with the predictions from the recent parametrizations within statistical limitations. The comparisons corroborate previous PHENIX measurements [4,48] that disfavor very large gluon polarization. The presented asymmetry measurements probe a range of approximately $0.05 \leq x_{\text{gluon}} \leq 0.2$ [16] of the interacting gluons.

[1]The DSSV curves in Fig. 5 were produced using source code graciously provided by the authors of Refs. [43,44].

V. SUMMARY AND CONCLUSIONS

Cross sections and double-helicity asymmetries for the midrapidity production of positive and negative inclusive charged hadrons at $\sqrt{s} = 62.4$ GeV are measured as a function of transverse momentum. The comparison of pQCD calculations with the measurements shows that the NLO estimations are consistent with cross-section results within a large scale uncertainty. NLL calculations with their reduced scale dependence are also consistent with the data, indicating that the threshold resummation of logarithmic terms is relevant in the kinematic region measured; however, the overprediction of the data by up to $\sim$50% if the NLL terms are included suggests that contributions from NNLO terms may also be important. This corroborates other recent results from PHENIX [18,48] with similar indications. The asymmetry results are the first measurements for charged hadron production in polarized $p + p$ collisions at $\sqrt{s} = 62.4$ GeV and are consistent with the asymmetries found using several other probes at different collision energies at RHIC [4,5,8,10,48,60]. Experimental measurements of a variety of processes covering a broad kinematic range are essential to advancing our understanding of QCD in hadronic interactions and nucleon structure, and the present measurements contribute towards that end.

ACKNOWLEDGMENTS

We thank the staff of the Collider-Accelerator and Physics Departments at Brookhaven National Laboratory and the staff of the other PHENIX participating institutions for their vital contributions. We also thank Daniel de Florian, Rodolfo Sassot, Marco Stratmann, Werner Vogelsang, and Federico Wagner for providing calculations, as well as Ted Rogers and Werner Vogelsang for valuable, in-depth discussions. We acknowledge support from the Office of Nuclear Physics in the Office of Science of the Department of Energy, the National Science Foundation, a sponsored research grant from Renaissance Technologies LLC, Abilene Christian University Research Council, Research Foundation of SUNY, and Dean of the College of Arts and Sciences, Vanderbilt University (USA), Ministry of Education, Culture, Sports, Science, and Technology and the Japan

Society for the Promotion of Science (Japan), Conselho Nacional de Desenvolvimento Científico e Tecnológico and Fundação de Amparo à Pesquisa do Estado de São Paulo (Brazil), Natural Science Foundation of China (P. R. China), Ministry of Education, Youth and Sports (Czech Republic), Centre National de la Recherche Scientifique, Commissariat à l'Énergie Atomique, and Institut National de Physique Nucléaire et de Physique des Particules (France), Bundesministerium für Bildung und Forschung, Deutscher Akademischer Austausch Dienst, and Alexander von Humboldt Stiftung (Germany), Hungarian National Science Fund, OTKA (Hungary), Department of Atomic Energy and Department of Science and Technology (India), Israel Science Foundation (Israel), National Research Foundation and WCU program of the Ministry Education Science and Technology (Korea), Ministry of Education and Science, Russian Academy of Sciences, Federal Agency of Atomic Energy (Russia), VR and the Wallenberg Foundation (Sweden), the U.S. Civilian Research and Development Foundation for the Independent States of the Former Soviet Union, the U.S.-Hungarian Fulbright Foundation for Educational Exchange, and the U.S.-Israel Binational Science Foundation.

[1] R. K. Ellis, H. Georgi, M. Machacek, H. D. Politzer, and G. G. Ross, Phys. Lett. **78B**, 281 (1978).
[2] J. C. Collins, D. E. Soper, and G. Sterman, Nucl. Phys. **B308**, 833 (1988).
[3] D. de Florian and W. Vogelsang, Phys. Rev. D **71**, 114004 (2005).
[4] A. Adare *et al.* (PHENIX Collaboration), Phys. Rev. Lett. **103**, 082002 (2009).
[5] B. I. Abelev *et al.* (STAR Collaboration), Phys. Rev. D **80**, 111108(R) (2009).
[6] A. Adare *et al.* (PHENIX Collaboration), Phys. Rev. D **84**, 012006 (2011).
[7] S. S. Adler *et al.* (PHENIX Collaboration), Phys. Rev. Lett. **97**, 052301 (2006).
[8] B. I. Abelev *et al.* (STAR Collaboration), Phys. Rev. Lett. **97**, 252001 (2006).
[9] S. S. Adler *et al.* (PHENIX Collaboration), Phys. Rev. Lett. **98**, 012002 (2007).
[10] J. Adams *et al.* (STAR Collaboration), Phys. Rev. Lett. **92**, 171801 (2004).
[11] I. Arsene *et al.* (BRAHMS Collaboration), Phys. Rev. Lett. **98**, 252001 (2007).
[12] M. Bonesini *et al.* (WA70 Collaboration), Z. Phys. C **42**, 527 (1989).
[13] D. L. Adams *et al.* (Fermilab E704 Collaboration), Phys. Lett. B **261**, 197 (1991).
[14] D. L. Adams *et al.* (Fermilab E704 Collaboration), Phys. Lett. B **336**, 269 (1994).
[15] L. Apanasevich *et al.* (Fermilab E706 Collaboration), Phys. Rev. D **68**, 052001 (2003).
[16] D. de Florian, W. Vogelsang, and F. Wagner, Phys. Rev. D. **76**, 094021 (2007).
[17] L. G. Almeida, G. F. Sterman, and W. Vogelsang, Phys. Rev. D **80**, 074016 (2009).
[18] A. Adare *et al.* (PHENIX Collaboration), Phys. Rev. C **83**, 064903 (2011).
[19] D. de Florian, R. Sassot, and M. Stratmann, Phys. Rev. D **76**, 074033 (2007).
[20] D. de Florian, R. Sassot, and M. Stratmann, Phys. Rev. D **75**, 114010 (2007).
[21] S. S. Adler *et al.* (PHENIX Collaboration), Phys. Rev. C **77**, 014905 (2008).
[22] S. S. Adler *et al.* (PHENIX Collaboration), Phys. Rev. C **69**, 034910 (2004).
[23] I. Alekseev *et al.*, Nucl. Instrum. Methods Phys. Res., Sect. A **499**, 392 (2003).
[24] G. Bunce, N. Saito, J. Soffer, and W. Vogelsang, Annu. Rev. Nucl. Part. Sci. **50**, 525 (2000).
[25] S. D. Bass, Rev. Mod. Phys. **77**, 1257 (2005).
[26] J. Ashman *et al.* (European Muon Collaboration), Phys. Lett. B **206**, 364 (1988).
[27] P. L. Anthony *et al.* (E142 Collaboration), Phys. Rev. D **54**, 6620 (1996).
[28] K. Abe *et al.* (E154 Collaboration), Phys. Rev. Lett. **79**, 26 (1997).
[29] K. Ackerstaff *et al.* (HERMES Collaboration), Phys. Lett. B **404**, 383 (1997).
[30] K. Abe *et al.* (E143 Collaboration), Phys. Rev. D **58**, 112003 (1998).
[31] B. Adeva *et al.* (Spin Muon Collaboration), Phys. Rev. D **58**, 112001 (1998).
[32] P. L. Anthony *et al.* (E155 Collaboration), Phys. Lett. B **493**, 19 (2000).
[33] X. Zheng *et al.* (JLab Hall A Collaboration), Phys. Rev. C **70**, 065207 (2004).
[34] K. V. Dharmawardane *et al.* (CLAS Collaboration), Phys. Lett. B **641**, 11 (2006).
[35] V. Y. Alexakhin *et al.* (COMPASS Collaboration), Phys. Lett. B **647**, 8 (2007).
[36] A. Airapetian *et al.* (HERMES Collaboration), Phys. Rev. D **75**, 012007 (2007).
[37] M. Glück, E. Reya, M. Stratmann, and W. Vogelsang, Phys. Rev. D. **63**, 094005 (2001).
[38] J. Blümlein and H. Böttcher, Nucl. Phys. **B841**, 205 (2010).
[39] E. Leader, A. V. Sidorov, and D. B. Stamenov, Phys. Rev. D **82**, 114018 (2010).
[40] M. G. Alekseev *et al.* (COMPASS Collaboration), Phys. Lett. B **693**, 227 (2010).
[41] A. Airapetian *et al.* (HERMES Collaboration), Phys. Rev. D **71**, 012003 (2005).
[42] W. Vogelsang (private communication).
[43] D. de Florian, R. Sassot, M. Stratmann, and W. Vogelsang, Phys. Rev. Lett. **101**, 072001 (2008).

[44] D. de Florian, R. Sassot, M. Stratmann, and W. Vogelsang, Phys. Rev. D **80**, 034030 (2009).
[45] K. Adcox *et al.* (PHENIX Collaboration), Nucl. Instrum. Methods Phys. Res., Sect. A **499**, 469 (2003).
[46] K. Adcox *et al.* (PHENIX Collaboration), Nucl. Instrum. Methods Phys. Res., Sect. A **499**, 489 (2003).
[47] A. Adare *et al.* (PHENIX Collaboration), Phys. Rev. Lett. **97**, 252002 (2006).
[48] A. Adare *et al.* (PHENIX Collaboration), Phys. Rev. D **79**, 012003 (2009).
[49] A. Drees and S. White, Conf. Proc. C **100523**, MOPEC013 (2010) [http://inspirehep.net/record/870248].
[50] A. Drees, B. Fox, Z. Xu, and H. Huang, Conf. Proc. C **030512**, 1688 (2003) [http://inspirehep.net/record/641222].
[51] I. Nakagawa *et al.*, AIP Conf. Proc. **980**, 380 (2008).
[52] H. Okada *et al.*, Phys. Lett. B **638**, 450 (2006).
[53] S. S. Adler *et al.* (PHENIX Collaboration), Phys. Rev. Lett. **95**, 202001 (2005).
[54] B. Alper *et al.* (ISR-British-Scandinavian Collaboration), Nucl. Phys. **B87**, 19 (1975).
[55] D. Drijard *et al.* (CERN-Dortmund-Heidelberg-Warsaw Collaboration), Z. Phys. C **12**, 217 (1982).
[56] GEANT 3.2.1, CERN Program Library (1993), http://wwwasdoc.web.cern.ch/wwwasdoc/pdfdir/geant.pdf.
[57] D. de Florian and F. Wagner (private communication).
[58] A. D. Martin, R. G. Roberts, W. J. Stirling, and R. S. Thorne, Eur. Phys. J. C **28**, 455 (2003).
[59] S. S. Adler *et al.* (PHENIX Collaboration), Phys. Rev. Lett. **91**, 072303 (2003).
[60] A. Adare *et al.* (PHENIX Collaboration), Phys. Rev. D. **76**, 051106 (2007).
[61] C. A. Aidala, F. Ellinghaus, R. Sassot, J. P. Seele, and M. Stratmann, Phys. Rev. D **83**, 034002 (2011).
[62] J. Pumplin, D. R. Stump, J. Huston, H. L. Lai, P. M. Nadolsky, and W. K. Tung, J. High Energy Phys. 07 (2002) 012.